Reduced graphene oxide porous films containing SiC whiskers for constructing multilayer electromagnetic shields

LI Jing*, Qi Yi-quan, ZHAO Shi-xiang, QIU Han-xun, YANG Jun-he, YANG Guang-zhi*

(*School of Materials and Chemistry*, *University of Shanghai for Science and Technology*, *Shanghai* 200093, *China*)

Abstract: Developing lightweight and flexible thin films for electromagnetic interference (EMI) shielding is of great importance. Porous thin films of reduced graphene oxide containing SiC whiskers (SiC@RGO) for EMI shielding were prepared by a two-step reduction of graphene oxide (GO), in which the two steps were chemical reduction by HI and the solid phase microwave irradiation. A significant increase of the film thickness from around 20 to 200 μm was achieved due to the formation of a porous structure by gases released during the 3 s of solid phase microwave irradiation. The total shielding effectiveness (SE_T) and the reflective SE (SE_R) of the SiC@RGO porous thin films depended on the GO/SiC mass ratio. The highest SE_T achieved was 35.6 dB while the SE_R was only 2.8 dB, when the GO/SiC mass ratio was 4∶1. The addition of SiC whiskers was critical for the multi-reflection, interfacial polarization and dielectric attenuation of EM waves. A multilayer film with a gradient change of SE values was constructed using SiC@RGO porous films and multi-walled carbon nanotubes buckypapers. The highest SE_T of the multilayer films reached 75.1 dB with a SE_R of 2.7 dB for a film thickness of about 1.5 mm. These porous SiC@RGO thin films should find use in multilayer or sandwich structures for EMI absorption in packaging or lining.

Key words: Graphene; Thin films; Silicon carbide whiskers; Electromagnetic interference shielding

1 Introduction

Carbon-based electromagnetic interference (EMI) shielding materials feature low density, diverse forms and tunable properties. Electrical conductivity of carbon materials has a wide range, depending on their crystal structures, chirality, oxidation degree, etc[1,2]. Compared to metal materials, carbon-based materials give the opportunity to construct lightweight, flexible, absorption-dominated EMI shielding materials[3].

Graphene-based thin films can be considered as a two-dimensional (2D) assembly of graphene layers which can be applied as the core layer in sandwich structure, packaging and lining materials for EMI shielding purpose[4,5]. Graphene oxide (GO) with a large number of oxygen-containing functional groups can be easily dispersed in water and aligned in thin films by liquid casting, vacuum filtration and electrodeposition. EMI shielding effects can be realized by restoring the electrical conductivity of the thin films upon reduction. However, the high electrical conductivity of reduced GO (RGO) may promote the reflection of electromagnetic (EM) radiation, resulting in reduction in absorption[4] because the reflection of EM radiations is a result of the interactions between the EM waves and free charges of carbon materials[6]. Iodine-doped RGO papers with an electrical conductivity of 10^3 S/cm showed an EMI shielding effectiveness (SE) of 52.2 dB and SE reflection (SE_R) of 18.6 dB[7], which may cause secondary EMI pollution.

RGO-based composite thin films were designed to improve the absorption of EMI. The addition of magnetic and semiconductive materials can promote EM attenuation, such as Fe_3O_4[8], MnO[9] and SiC[10]. SiC whiskers/MnO/RGO composites were constructed for improving EMI absorption, where SiC whiskers can dielectrically attenuate EM waves as a semiconductor[11]. Synergistic effects on EMI shielding were expected by combining SiC with an conductive phase, such as carbon nanotube-carbon fiber/SiC[12] and SiC/MXene/polymer [13] composites.

Compared with 2D composite thin films with RGO layers, three-dimensional (3D) assembly of

Received date: 2024-01-31; **Revised date:** 2024-04-19

Corresponding author: LI Jing, Professor. E-mail: lijing6080@usst.edu.cn;
YANG Guang-zhi, Professor. E-mail: yanggzh@usst.edu.cn

graphene or RGO layers provided graphene monoliths with high porosity and low density. The EMI SE of RGO monoliths mainly came from the direct absorption and the absorption of multiple-reflected EM radiations, which were facilitated by their high porosity and large surface area[6]. The EMI SE of RGO monoliths can also be tuned by composite design, such as infiltration of conductive polymers[6], Fe_3O_4, carbon nanotubes[14] and MXene[15]. Porous structure was also reported for MXene/RGO flexible thin film, which had a total SE（SE_T）of 55.2 dB with a thickness of only 32 μm, but the high electrical conductivity of 10^3 S/cm, resulting in a SE_R value of around 20 dB[16].

Construction of multilayer composites was another strategy to improve the absorption of EM radiation. The multilayer structure with varying EMI SE of each layer could trap and attenuate the entered EM waves by repeated adsorption, reflection, and scattering in the composite film. The EMI SE of the Fe_3O_4@RGO/MWCNT/waterborne polyurethane (WPU) multilayer composites reached 35.9 dB using MWCNT/WPU as the reflection layer[17]. The gradients and sequence of the Fe_3O_4@RGO layers played an important role on the absorption/reflection ratio. A reflection layer with high electrical conductivity was usually employed to reduce the EM transmission, including Ag/glass fibers[18] and MWCNT buckypaper[19,20]. EMI SE of over 100 dB was obtained by a sandwich structure of multilayer buckypaper and wave-transmitting layers with a SE_R of around 15 dB and a thickness of over 20 mm[20].

In this study, SiC@RGO porous thin films were fabricated with the assistance of solid phase microwave irradiation. The amount of SiC whiskers in the SiC@RGO thin films was critical for generating the porous structure and controlling the reduction degree of RGO. The absorption-dominated EMI shielding was realized by the dielectric attenuation of EM waves by SiC, the multi-reflection in the porous thin films and the interfacial polarization between SiC and RGO. In addition, a MWCNT buckypaper was adhered to the SiC@RGO porous film for further improving EMI while remaining the flexibility.

2 Experimental

2.1 Preparation of SiC@RGO

4 g SiC whiskers (Hebei Chuancheng Metal Materials) was dispersed in 40 mL H_2O_2 under stirring, followed by washing, filtration and drying. Then, 3-triethoxysilylpropylamine was hydrolyzed at a concentration of 2% when the pH value was adjusted to 4 by acetic acid. 4 g SiC powder reacted with 60 mL silane solution for 24 h at room temperature. The silane-treated SiC was obtained after washing and filtration. GO (5 mg·mL^{-1}, Anguqiang Graphene Technology) was mixed with the treated SiC by sonication for 30 min, The mixture was casted in a polytetrafluoroethylene Petri dish and dried in the oven at 60 °C for 24 h to prepare SiC@GO thin films. The GO/SiC weight ratios were 12∶0, 12∶1, 12∶2, 12∶3 and 12∶4 for different samples.

The SiC@GO films were reduced firstly by HI (55%–57%) in a hydrothermal autoclave at 90 °C for 1 h. After repeated washing and drying, the thin films were then put into a microwave oven (M1-L213B, output 700 W) for 3 s for secondary reduction to obtain SiC@RGO thin films. The samples were named SiC@RGO0, SiC@RGO1, SiC@RGO2, SiC@RGO3 and SiC@RGO4, according to the SiC content.

2.2 Fabrication of SiC@RGO/buckypaper multilayer composites

MWCNTs were dispersed in DI water at a concentration 0.5 mg/mL using 0.5% (mass fraction) of Triton X-100 as the dispersant in an ultrasonic homogenizer (JY96-IIN) for 30 min. The suspension was then filtered using a cellulose filter membrane (0.22 μm pore size) and the buckypaper was obtained after washing and drying. The SiC@RGO thin films were adhered to the buckypaper with WPU (WPU, New City Engineering Plastics) by a glass rod. The fabrication procedure of SiC@RGO/buckypaper multilayer composites was shown in Fig. 1.

2.3 Characterization

The morphology of the thin films was investigated by scanning electron microscopy (SEM, FEI

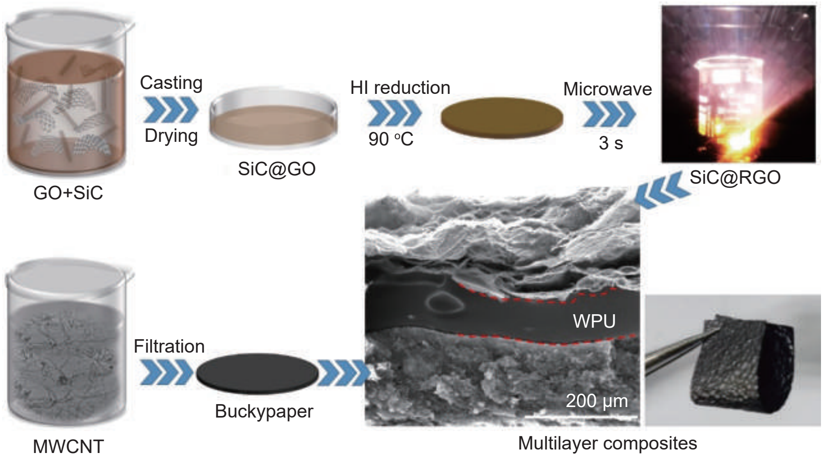

Fig. 1 Fabrication procedure of SiC@RGO/buckypaper multilayer composites

Quanta FEG). X-ray diffraction (XRD, D8 Advance, Bruker), Raman spectrometer (LabRAM, Horiba) and Fourier infrared spectrometer (FTIR, Spectrum 100 PerkinElmer) were employed to characterize the material structure. The thermal stability of the thin films was studied by thermal gravimetric analyzer (TGA, Pyris 1). The specific surface area of the porous thin films was analyzed by the Brunauer-Emmett-Teller（BET）method using ASAP2020. The electrical conductivity and the S (S11, S21, S22, S12) parameters of the thin films were characterized using a four-probe system (RTS-9, MTI Corporation) and a vector network analyzer (Keysight E5063A), respectively. The S parameters allow the calculation of the total SE (SE_T), absorption SE (SE_A) and reflection SE (SE_R), according to the Equation 1-6, where the multiple internal reflections (SE_M) is negligible if EMI $SE_T \geqslant$ 10 dB[6,17].

$$R = |S_{11}|^2 = |S_{22}|^2 \tag{1}$$

$$T = |S_{21}|^2 = |S_{12}|^2 \tag{2}$$

$$A = 1 - R - T \tag{3}$$

$$SE_R = -10\lg(1-R) \tag{4}$$

$$SE_A = -10\lg[T/(1-R)] \tag{5}$$

$$SE_T = SE_R + SE_A + SE_M \tag{6}$$

3 Results and discussion

3.1 Structure and morphology of SiC@RGO thin films

Fig. 2a shows the FTIR spectra of SiC before and

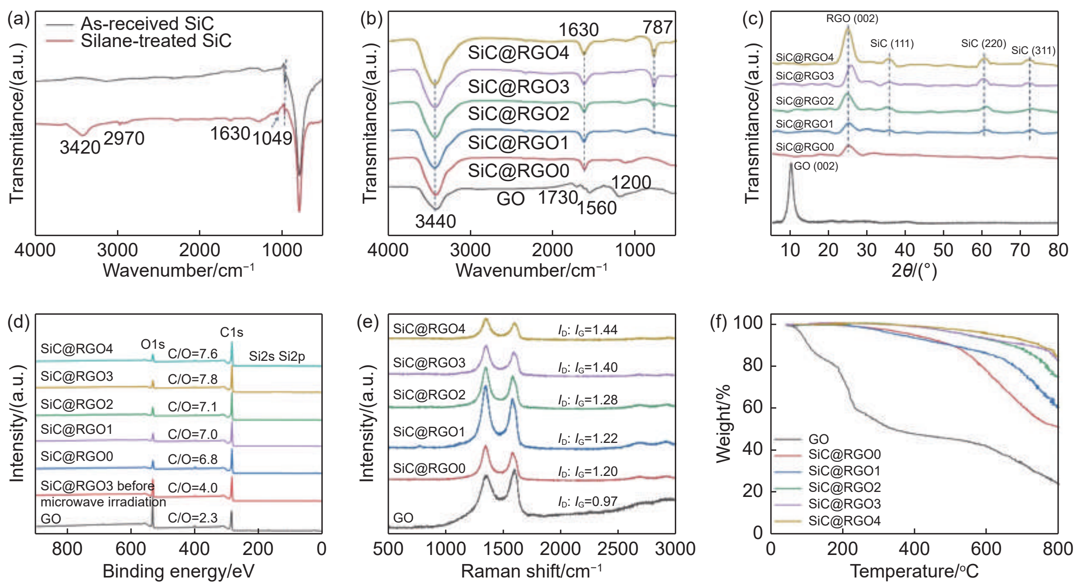

Fig. 2 FTIR spectra of (a) SiC whiskers before and after silanization. (b) FTIR spectra, (c) XRD patterns, (d) XPS spectra, (e) Raman spectra and (f) TGA results of GO and SiC@RGO thin films

after the silane-treatment, where the strong peak at 787 cm^{-1} came from C—Si bonding of SiC whiskers. The silane-treated SiC showed extra peaks at 3 420, 2 970, 1 630 and 1 049 cm^{-1}, corresponding to N—H, C—H, NH_2 and Si—O—C stretching vibration, respectively, suggesting the grafting of aminosilane molecules on SiC. Electrostatic interaction was enhanced between the amino groups on SiC and the carboxyl groups on GO during the assembly of SiC@GO thin films.

The FTIR spectra of SiC@RGO thin films were shown in Fig. 2b. The characteristic peaks of GO included 3 440 cm^{-1} (—OH), 1 730 cm^{-1} (C=O), 1 560 cm^{-1} (C=C) and 1 200 cm^{-1} (C—O). The peaks of C=O and C—O disappeared upon reduction of GO, while the peak at 1 630 cm^{-1} appeared and attributed to the restore of C=C bonding. With increasing the content of SiC, the peak of C—Si at 787 cm^{-1} became strong.

Upon reduction, the peak of GO (002) was moved from 10° to 25° of RGO (002) due to the decreased interlayer distance (Fig. 2c). The characteristic peaks of β-SiC at 35°, 60° and 71.8° appeared with the addition of SiC whiskers, corresponding to the (111), (220) and (311) crystal planes, respectively[11]. It's worth noting that the peak intensity of RGO (002) increased with the content of SiC in SiC@RGO thin films, indicating the improved crystallinity and reduction degree of RGO. Table 1 listes the full width at half maximum (FWHM) values and the crystal size along RGO (002) plane calculated according to Scherrer equation. The FWHM of the RGO (002) peaks decreased and the crystal size increased with increasing the SiC content, indicating that the reduction degree of RGO was improved until the SiC content was 20%. The addition of SiC facilitated the microwave absorption and the SiC@RGO thin film sparked during the solid phase microwave irradiation for less than 1 s, as shown in Fig. 1, while the sparks were not observed for SiC@RGO0 thin film. A large amount of heat was generated during the strong arc discharge in a few seconds[21-23]. As a result, GO was quickly reduced and the reduction degree could be tailored by the SiC content.

To confirm the effect of SiC content on the reduction degree of GO, XPS spectra were shown in Fig. 2d. The C/O ratio clearly increased with the SiC content of SiC@RGO thin films and reached the highest value of 7.8 when SiC content was 20%, as listed in Table 1. The SiC@RGO thin films were reduced by a two-step reduction procedure, which was chemical reduction by HI and heat reduction by the solid phase microwave irradiation. Reduction by HI increased the C/O of GO from 2.3 to 4, and the solid phase microwave irradiation increased the C/O ratio from 4 to 7.8 when the SiC content was 20%. Further increase of the SiC content did not promote the reduction degree, which was consistent with the XRD results. Rapid reduction of GO into pristine graphene by 1–2 s of microwaves irradiation has been reported[23], where GO showed strong absorption capacity due to the existence of π–π conjugated regions and polyaromatic domains[24]. SiC offered extra “heat points” as the dispersed phase in the thin films because its high dielectric constant facilitated the transformation of microwave energy to heat[25].

Raman spectra of SiC@RGO thin films showed *D* and *G* peaks of graphene at 1 350 and 1 580 cm^{-1} (Fig. 2e), corresponding to the defects and sp^2 carbon, respectively. The intensity ratio of the *D* and *G* peaks

Table 1 FWHM, crystal size, C/O ratio, I_D/I_G, surface area and average pore size of the SiC@RGO thin films

Samples	FWHM/(°)	Crystal size/nm	C/O	$I_D : I_G$	Weight loss at 800 °C	Surface area/(m^2/g)	Pore size/nm
GO	–	–	2.3	0.97	76.1%	–	–
SiC@RGO0	3.444	2.371	6.8	1.20	49.0%	24.28	9.24
SiC@RGO1	2.770	2.948	7.0	1.22	39.9%	20.89	13.53
SiC@RGO2	2.726	2.993	7.1	1.28	25.7%	15.06	18.15
SiC@RGO3	2.185	3.742	7.8	1.40	17.4%	12.87	16.85
SiC@RGO4	2.394	3.410	7.6	1.44	15.2%	8.18	28.89

(I_D/I_G) increased gradually with the SiC content (Table 1), suggesting the microwave absorption promoted the formation of defects in the basal plane of RGO. Thermal stability of the thin films increased with the reduction degree (Fig. 2f). The weight loss of GO was 76.1% due to the decomposition of oxygen-containing functional groups at high temperature. The weight loss was reduced significantly to 15.2% with increasing the SiC content. The SiC@RGO3 and SiC@RGO4 thin films kept stable until 500 °C, suggesting a high end-use temperature.

Morphology of the thin films with different SiC contents was shown in Fig. 3a-f before and after the microwave irradiation. Before the microwave irradiation, a multilayer structure was featured and the thickness of the thin films increased slightly with the SiC content, ranging from 17 to 23 μm. After the microwave irradiation, a porous structure was featured and a significant increase of the film thickness was observed to 100–200 μm. The largest distance between the neighboring graphene layers was observed over 50 μm. The porous structure was due to the thermal shock generated by only 3 s of solid phase microwave irradiation, which removed a large amount of oxygen-containing functional groups and released small molecules suddenly.

The average pore size of the RGO/SiC thin films (Table 1) increased with the SiC content, agreeing well with the SEM observation, although the specific surface area decreased because SiC has a higher density of 3.2 g/cm^3 than RGO. Porous structure may lead to fragile materials. This was the reason why the two-step reduction of SiC@GO was employed. The chemical reduction by HI will reduce the concentration of oxygen-containing functional groups to a centain extent and the residue groups were reduced to release small molecules, which expanded the layer space and generated pores during the microwave irradiation, so that the flexibility and porosity of the SiC@RGO thin film were balanced.

3.2 EMI shielding performance of the SiC@RGO thin films

The electrical conductivities of SiC@RGO films before and after the microwave irradiation were shown in Fig. 4. The electrical conductivity of pure RGO films reached 14.6 S/cm after the reduction by HI, and then decreased to 5.2 S/cm after the microwave irradiation. For all the SiC@RGO thin films, the microwave irradiation decreased the electrical conductivity for over 50%. However, the microwave irradiation increased the degree of reduction as proven by the C/O ratio shown in Fig. 2d. The reason for the decreased electrical conductivity was the significant amount of pores generated by microwave irradiation, which reduced the electrical contacts between neighboring graphene layers. The electrical conductivity of the SiC@RGO films decreased consistently with the content of SiC before the microwave irradiation because the SiC whiskers were nonconductive. However, the electrical conductivities of SiC@RGO1

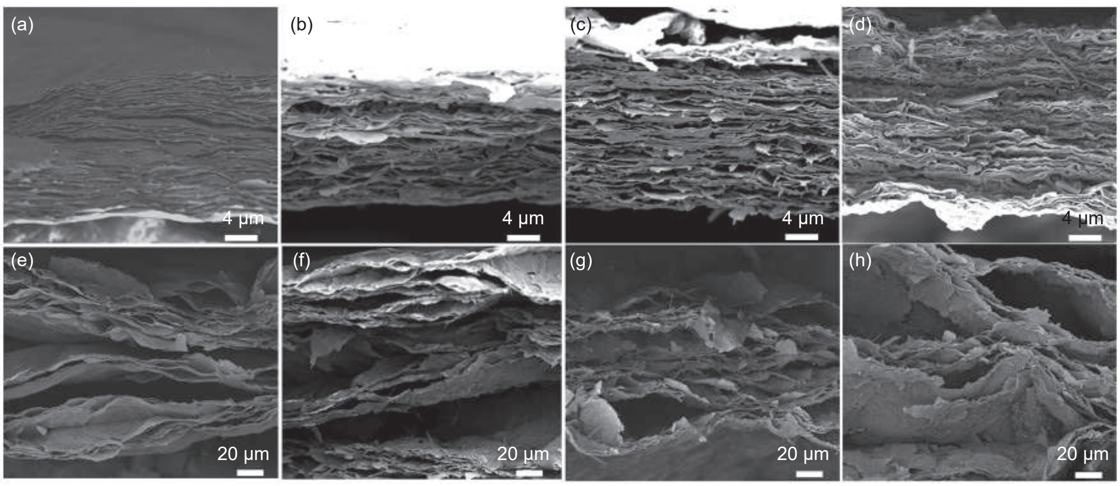

Fig. 3　Cross-section morphology of SiC@RGO0, SiC@RGO1, SiC@RGO2 and SiC@RGO3 thin films (a-d) before and (e-f) after microwave irradiation

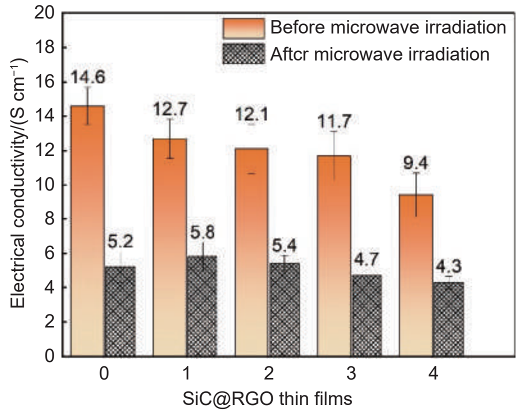

Fig. 4 Electrical conductivities of SiC@RGO thin films before and after microwave irradiation

and SiC@RGO2 were higher a little bit than SiC@RGO0 after the microwave irradiation because 3 effects were combined, namely the reduction degree of RGO, the SiC content and the porosity.

The EMI SE of the thin films was measured in the frequency range of 8.2–12.4 GHz (Fig. 5). The SE_T increased with the SiC content and reached a maximum value of 29.5 dB for SiC@RGO3 before the microwave irradiation. The improvement was attributed completely to the increase of SE_A, which was dominated and counted for 27.1 dB, while the SE_R was only 2.4 dB. The addition of SiC promoted significantly the absorption of the EM waves by dielectric attenuation, which was consistent with its effect on microwave absorption. Excessive amount of SiC reduced the EMI SE of the SiC@RGO4 thin films probably due to its agglomeration.

The SE_T of the thin film was further improved for over 20% by the microwave irradiation, as shown in Fig. 6, although the electrical conductivity of the thin films was reduced. The reasons for the significant improvement lied in two aspects, one is the reduction degree of RGO, the other is the generation of the pores in the films. The improvement was again mainly attributed to the SE_A, noting that the SE_R values were barely changed before and after the microwave irradiation. The enhanced reduction degree of RGO facilitated the interaction between the EM waves and free charges on each RGO layers in a highly localized scale. In a larger scale, the EM waves underwent an absorption and multi-reflection between neighboring RGO layers and the walls of the pores. The SE_T values were higher than 30 dB for the porous thin films with SiC. The SE_T of SiC@RGO3 thin films reached

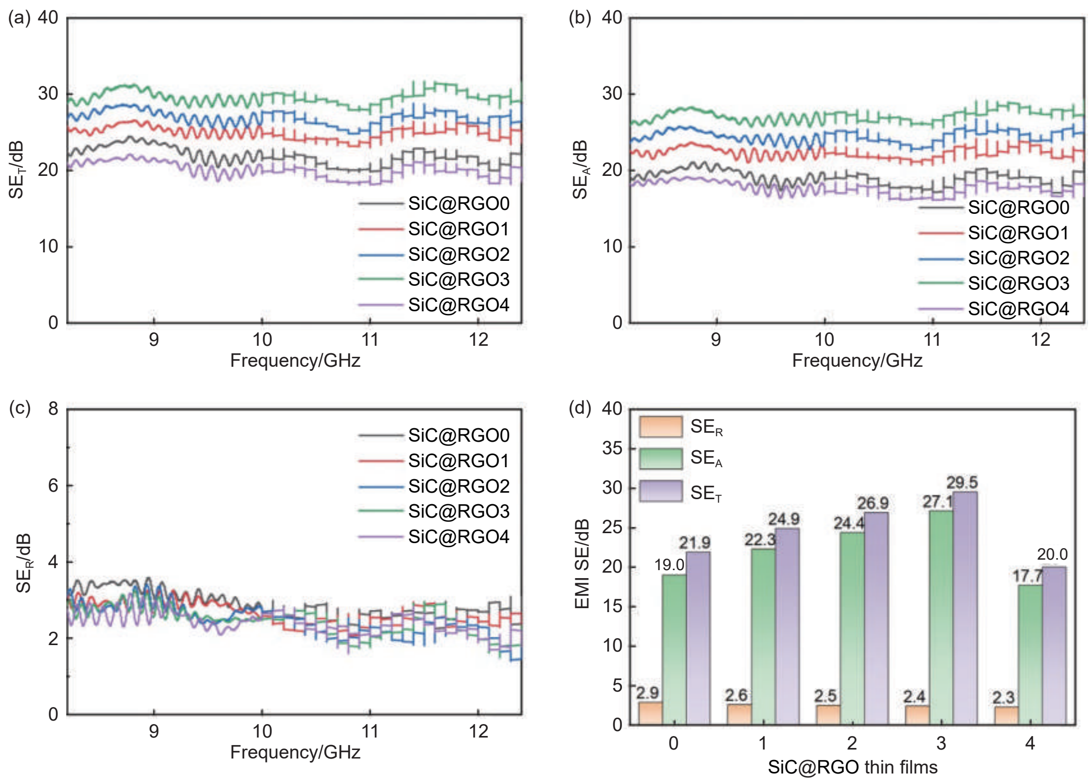

Fig. 5 (a) SE_T, (b) SE_A, (c) SE_R and (d) average SE values of the SiC@RGO thin films before the microwave irradiation

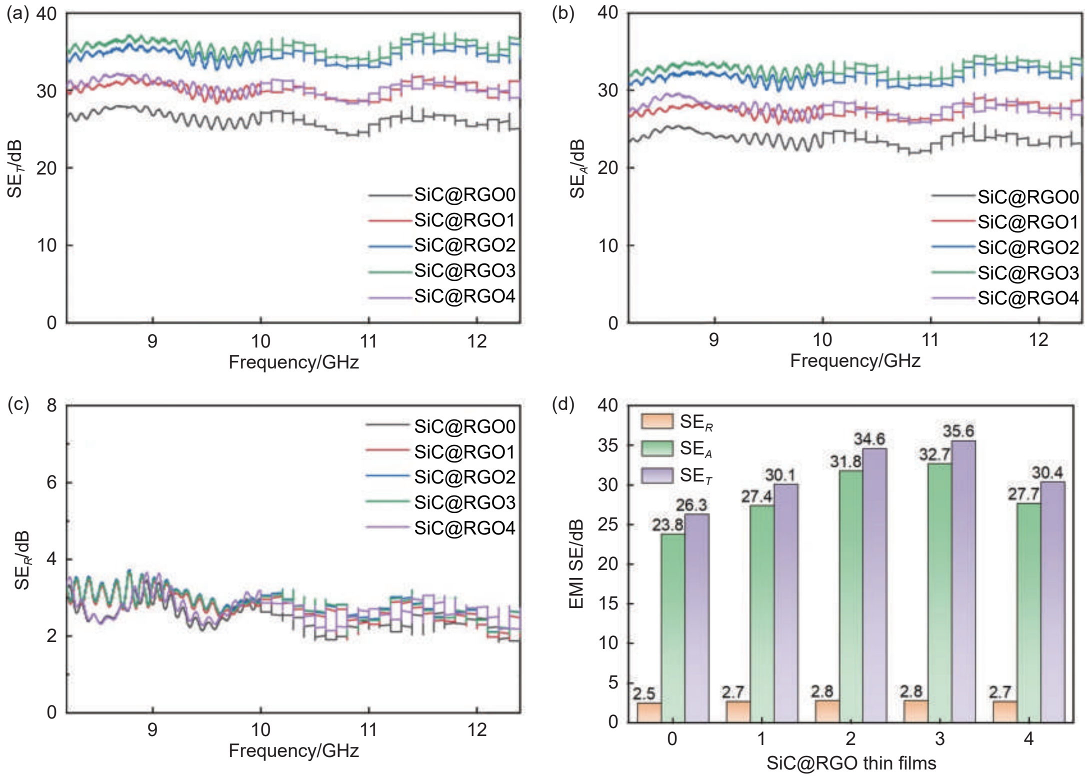

Fig. 6　(a) SE$_T$, (b) SE$_A$, (c) SE$_R$ and (d) average SE values of the SiC@RGO thin films after the microwave irradiation

the highest value of 35.6 dB with a SE$_A$ of 32.7 dB, where the effects of SiC had 3 aspects: (1) Improving the reduction degree of RGO, (2) Promoting the porous structure of the thin films, (3) Introducing dielectric attenuation of EM waves.

3.3　Morphology and properties of multilayer composites

Multilayer composites were constructed, as shown in Fig. 7, using MWCNT buckypaper (Fig. 7b) as the reflection layer and WPU with a thickness of around 80 μm (Fig. 1) as the adhesive. Three layers of SiC@RGO thin films were stacked in a sequence (Fig. 7a), where SiC@RGO2, SiC@RGO3, SiC@RGO4 were chosen because they had relatively low electrical conductivities and high SE$_T$ values. The thickness of the multilayer composites was slightly over 1.5 mm (Fig. 7c) with a good flexibility (Fig. 1).

To determine the optimal sequence of the 3 SiC@RGO layers, the EMI SE values were compared for all the arrangement without the MWCNT buckypaper (Fig. 8). Apparently, the SE$_T$ of the composites varied with the arrangement sequence. The highest SE$_T$ of 66.3 dB and the lowest SE$_R$ of 2.5 dB were achieved when the 3 layers of SiC@RGO thin films were arranged in the order of increasing electrical conductivity. When the EM waves were incident from the SiC@RGO layer with lower conductivity, it tended to have a higher SE$_A$ and lower SE$_R$. The layer

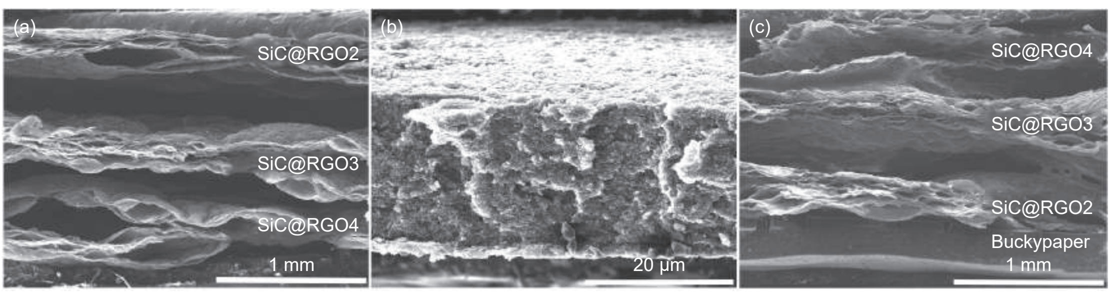

Fig. 7　Morphologies of (a) SiC@RGO2/3/4 stacking layers by WPU adhesives, (b) MWCNT buckypaper, and (c) multilayer composites of SiC@RGO4/3/2 and buckypaper as the reflection layers

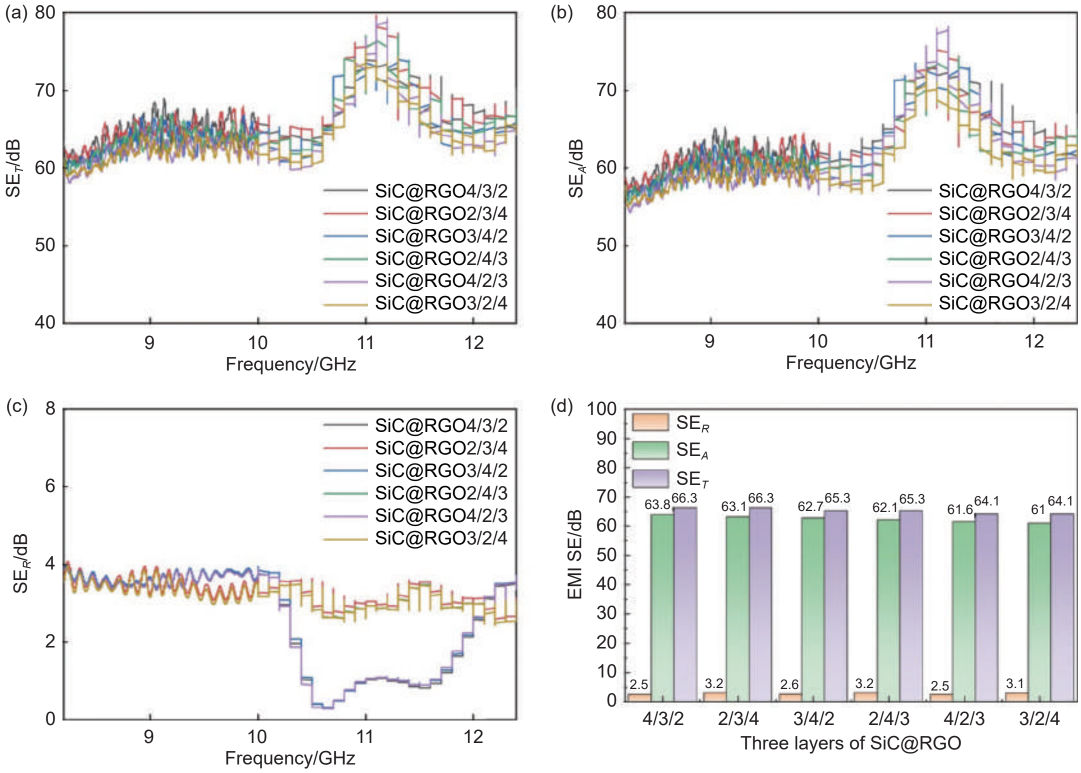

Fig. 8 (a) SE_T, (b) SE_A, (c) SE_R and (d) average SE values for all the stacking sequence of the 3 SiC@RGO layers

with higher conductivity should have higher reflection, which was more suitable for the bottom layer in the arrangement sequence.

With the optimal sequence of SiC@RGO4/3/2 and the MWCNT buckypaper as the reflection layer, their conductivity values were 4.3 S/cm, 4.7 S/cm, 5.4 S/cm and 9.0 S/cm from top to bottom. The SE_T and SE_R of the MWCNT buckypaper were 41.0 and 3.5 dB (Fig. 9a). Both the electrical conductivity and SE_R of the MWCNT buckypaper were slightly higher than the SiC@RGO layers, which gave an suitable material selection for the reflection layer to reduce the transmission the EM waves and match the impedance between neighboring layers. Thereafter, a 4-layer composite was constructed and its EMI SE was compared with a 2-layer composites with SiC@RGO3 and buckypaper (Fig. 9b, c). The SE_T of the 4-layer composite was 32% higher than the 2-layer composite and reached 75.1 dB, meeting the requirement of the high performance EMI shielding material, while the SE_R value of the 4-layer composite was slightly lower than that of the 2-layer composite.

As schematically shown in Fig. 10a, the top layer of SiC@RGO4 had the lowest conductivity and

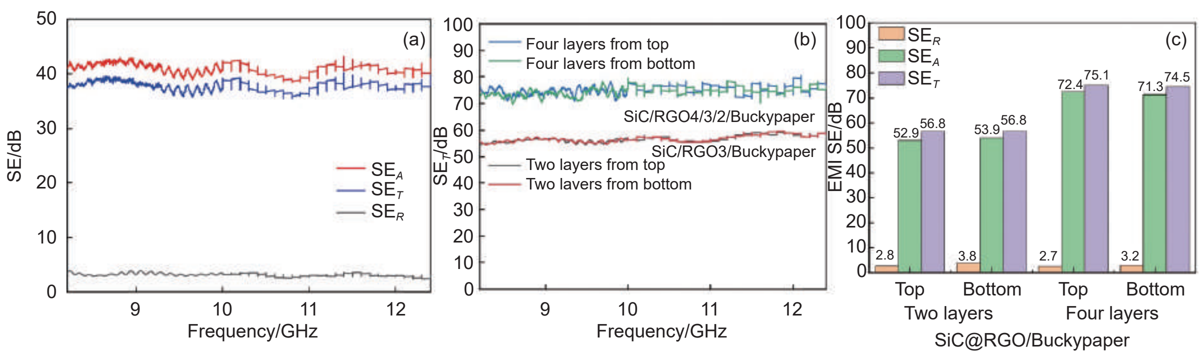

Fig. 9 (a) EMI SE of MWCNT buckypaper. (b) SE_T and (c) average SE values of the 2-layer and 4-layer composites with incident waves from top and bottom

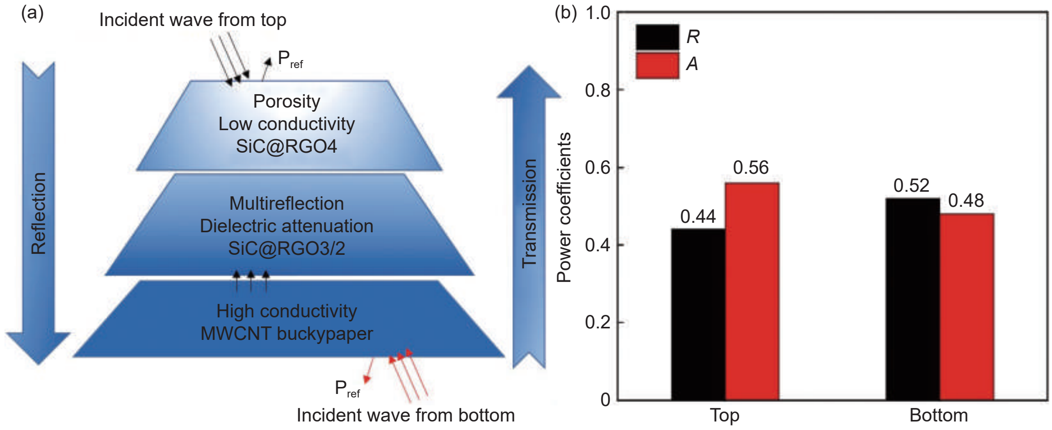

Fig. 10 (a) Mechanism for EMI shielding in the multilayer composites. (b) Average values of *R* and *A* for the multilayer composites with incident waves from top and bottom

highest average pore size, which gave an impedance matching layer and reduced the reflection[26]. In addition, the SiC in the top 3 layers provided not only porosity and dielectric attenuation, but also a large number of heterogeneous interfaces, which improved interfacial polarization. A dense buckypaper layer served to reflect EM waves, benefited from its high electrical conductivity[27]. The SE_T was increased by 13.3% when the MWCNT buckypaper was applied as shown in Fig. 8d and 9c, without much change of SE_R.

Again, the incident direction affected the portion of SE_A and SE_R, while the SE_T values were barely changed (Fig. 9c). The SE_R was 2.7 and 3.2 dB when the EM waves were incident from top and bottom layer, respectively. The reflection (*R*) and absorption (*A*) coefficients were calculated according to the Equation (1–3) (Fig. 10b). The transmission coefficient (*T*) can be neglected when the EMI SE was higher than 30 dB[17]. The A/R ratio was higher than 1 when the incident waves were from the top layer (SiC@RGO4), indicating an adsorption-dominated EMI shielding mechanism. Therefore, the top layer should have low conductivity and high porosity for trapping the EM waves. The transmitted EM waves interacted with the center layers (SiC@RGO3/2), which featured intermediate conductivity and high SE_A. The bottom layer (buckypaper) gave the highest conductivity to enhance the reflection and reduce transmission. Therefore, the interaction between the EM waves and the multilayer composites can be descripted as absorption/transmission (top) → absorption/multi-reflection (center) → reflection (bottom) → re-absorption/multi-reflection (center), which greatly improved the EMI shielding performance (Fig. 10a). A high SE_T value of over 70 dB has been reported for graphene/WPU composite film with a thickness of 0.9 mm[28], while our multilayer composite films featured the absorption-dominated EMI shielding with a low SE_R value of 2.7 dB.

4 Conclusions

SiC@RGO porous thin films were fabricated by a two-step reduction process, which was chemical reduced by HI and solid phase microwave irradiated for only 3 s. The addition of SiC facilitated the absorption of the microwave, generated sparks and resulted in a high reduction degree of RGO and a large number of pores in the thin films. The electrical conductivity of the SiC@RGO thin films decreased by over 50% while the SE_T and SE_A increased by over 20% upon the microwave irradiation. Meanwhile, the addition of 20% SiC whiskers increased the SE_T by 36.4%. These could be attributed to the multi-reflection, interfacial polarization, dielectric attenuation and impedance matching. Further, the multilayer composites were constructed by stacking the SiC@RGO thin films in a sequence and using the MWCNT buckypaper as the reflection layer. The highest SE_T reached 75.1 dB with a SE_R value of 2.7 dB when a thickness was about 1.5 mm. The sequence of the three SiC@RGO layers should be optimally arranged by increasing conductivity from top to bottom, so that a gradient change from transmission to reflection was achieved in addition to the effective absorption of multi-reflected EM waves. We hope the porous SiC@RGO thin films could be a promising material in designing multilayer or sandwich structure for use as EMI absorption packaging or lining materials.

References

[1] Wang Y Y, Zhang F, Li N, et al. Carbon-based aerogels and foams for electromagnetic interference shielding: A review[J]. Carbon, 2023, 205: 10-26.

[2] Li W, Gao M, Miao Y, et al. Recent progress in increasing the electromagnetic wave absorption of carbon-based materials[J]. New Carbon Materials, 2023, 38: 111-129.

[3] Zhang F, Li C, Zhang Y, et al. Facile preparation of large-scale expanded graphite/polydimethylsiloxane composites for highly-efficient electromagnetic interference shielding[J]. Journal of Materials Chemistry A, 2022, 10: 23145.

[4] Xia T, Cao J Y, Bissett M A, et al. Graphenization of graphene oxide films for strongly anisotropic thermal conduction and high electromagnetic interference shielding[J]. Carbon, 2023, 215: 118496.

[5] Tahalyani J, Akhtar M J, Kar K K. Flexible, stretchable, and thin films based on functionalized carbon nanofiber/graphene nanostructures for electromagnetic interference shielding[J]. ACS Applied Nano Materials, 2023, 6: 8178-8191.

[6] Wu Y, Wang Z, Liu X, et al. Ultralight graphene foam/conductive polymer composites for exceptional electromagnetic interference shielding[J]. ACS Applied Materials & Interfaces, 2017, 9: 9059-9069.

[7] Wan Y J, Zhu P L, Yu S H, et al. Graphene paper for exceptional EMI shielding performance using large-sized graphene oxide sheets and doping strategy[J]. Carbon, 2017, 122: 74-81.

[8] Kumar N, Kuanr B K. Single and double-layered tri-band microwave absorbing materials[J]. Ceramics International, 2023, 49: 32458-32469.

[9] Duan Y, Xiao Z, Yan X, et al. Enhanced electromagnetic microwave absorption property of peapod-like MnO@carbon nanowires[J]. ACS Applied Materials & Interfaces, 2018, 10: 40078-40087.

[10] Zhao Y, Zhang Y, Yang C, et al. Ultralight and flexible SiC nanoparticle-decorated carbon nanofiber mats for broad-band microwave absorption[J]. Carbon, 2021, 171: 474-483.

[11] Dong S, Zhang X, Li X, et al. SiC whiskers-reduced graphene oxide composites decorated with MnO nanoparticles for tunable microwave absorption[J]. Chemical Engineering Journal, 2020, 392: 123817.

[12] Cai Y, Li Y, Huang S, et al. Broadband electromagnetic shielding performance of carbon nanotube-carbon fibre/silicon carbide cross-scale laminated composites[J]. Ceramics International, 2022, 48: 26177-26187.

[13] Ma L, Hamidinejad M, Liang C, et al. Enhanced electromagnetic wave absorption performance of polymer/SiC-nanowire/MXene ($Ti_3C_2T_x$) composites[J]. Carbon, 2021, 179: 408-416.

[14] Liang C, Song P, Ma A, et al. Highly oriented three-dimensional structures of Fe_3O_4 decorated CNTs/reduced graphene oxide foam/epoxy nanocomposites against electromagnetic pollution[J]. Composites Science and Technology, 2019, 181: 107683.

[15] Hu B, Guo H, Li J, et al. Dual-encapsulated phase change composites with hierarchical MXene-graphene monoliths in graphene foam for high-efficiency thermal management and electromagnetic interference shielding[J]. Composites Part B-Engineering, 2023, 266: 110998.

[16] Tang X, Luo J, Hu Z, et al. Ultrathin, flexible, and oxidation-resistant MXene/graphene porous films for efficient electromagnetic interference shielding[J]. Nano Research, 2023, 16: 1755-1763.

[17] Sheng A, Ren W, Yang Y, et al. Multilayer WPU conductive composites with controllable electro-magnetic gradient for absorption-dominated electromagnetic interference shielding[J]. Composites Part A: Applied Science and Manufacturing, 2020, 129: 105692.

[18] Yang J, Liao X, Wang G, et al. Heterogeneous silicon rubber composite foam with gradient porous structure for highly absorbed ultra-efficient electromagnetic interference shielding[J]. Composites Science and Technology, 2021, 206: 108663.

[19] Kim M, Kim S, Seong Y C, et al. Multiwalled carbon nanotube buckypaper/polyacrylonitrile nanofiber composite membranes for electromagnetic interference shielding[J]. ACS Applied Nano Materials, 2021, 4(1): 729-738.

[20] Hu Y, Li D, Wu L, et al. Carbon nanotube buckypaper and buckypaper/polypropylene composites or high shielding effectiveness and absorption-dominated shielding material[J]. Composites Science and Technology, 2019, 181: 107699.

[21] Jiang W S, Yang C, Chen G X, et al. Preparation of high-quality graphene using triggered microwave reduction under an air atmosphere[J]. Journal of Materials Chemistry C, 2018, 6(7): 1829-1835.

[22] Sun Y, Qiu S, Fang Z, et al. Rapid synthesis of oxygen-deficient MoO_3-x-rGO composites for synergistic photothermal seawater desalination and photocatalytic sterilization[J]. ACS Sustainable Chemistry & Engineering, 2023, 11: 3359-3369.

[23] Voiry D, Yang J, Kupferberg J, et al. High-quality graphene via microwave reduction of solution-exfoliated graphene oxide[J]. Science, 2016, 353: 1413-1416.

[24] Hu H, Zhao Z, Zhou Q, et al. The role of microwave absorption on formation of graphene from graphite oxide[J]. Carbon, 2012, 50: 3267-3273.

[25] Tamang S, Aravindan S. 3D numerical modelling of microwave heating of SiC susceptor[J]. Applied Thermal Engineering, 2019, 162: 114250.

[26] Yang W, Yan L, Jiang B, et al. Crumpled nitrogen-doped porous carbon nanosheets derived from petroleum pitch for high-performance and flexible electromagnetic wave absorption [J], Industrial & Engineerng Chemistry Research , 2022, 61:

2799−2808.

[27] Yang W, Jiang B, Che S, et al. Research progress on carbon-based materials for electromagnetic wave absorption and the related mechanisms[J]. New Carbon Materials, 2021, 36: 1016-1033.

[28] Yang W, Bai H, Jiang B, et al. Flexible and densified graphene/waterborne polyurethane composite film with thermal conducting property for high performance electromagnetic interference shielding[J]. Nano Research, 2022, 15: 9926-9935.